Graphical Abstract

Grain size evolution in mantle convection models promotes continuous rather than episodic tectonics

Antonio Manjón-Cabeza Córdoba, Tobias Rolf, Maëlis Arnould

Highlights

Grain size evolution in mantle convection models promotes continuous rather than episodic tectonics

Antonio Manjón-Cabeza Córdoba, Tobias Rolf, Maëlis Arnould

- We systematically investigate self-consistent planetary geodynamic models with grain size evolution
- Tectonic regime diagnostics, such as surface mobility or internal temperature, depend on grain size evolution
- Including grain size evolution alters the transition between episodic and continuous mobile lid, but not the boundary to the stagnant lid

Grain size evolution in mantle convection models promotes continuous rather than episodic tectonics

Antonio Manjón-Cabeza Córdoba[a,b,c], Tobias Rolf[b,d], Maëlis Arnould[e]

[a] *University College London, Department of Earth Sciences, 5 Gower Place, London, WC1E 6BS, U.K.*
[b] *The Centre for Earth Evolution and Dynamics (CEED), Universitetet i Oslo, P.O. Box 1028 Blindern, Oslo, N-0315, Norway*
[c] *Instituto Andaluz de Ciencias de la Tierra (UGR-CSIC), Avda. de las Palmeras 4, Granada, 18100, Spain*
[d] *Institute of Geophysics, University of Münster, Corrensstrasse 24, Münster, 48149, Germany*
[e] *University of Lyon, UCBL, ENSL, UJM, CNRS 5276, Laboratoire de Géologie de Lyon - Terre, Plànetes, Environnement, Camps de la DOUA Bâtiement Géode 2 Rue Raphaël Dubois, Lyon, 69622, France*

Abstract

A long-persistent caveat of geodynamic models with Earth-like tectonic behavior is the need of an 'ad hoc' yield stress lower than any laboratory-inferred rock strength. Grain size reduction due to dynamic recrystallization provides local weak zones in the lithosphere thereby promoting lithospheric breakdown and continuous mobile-lid tectonics. Grain growth should instead (re-)strengthen the lithosphere and inhibit this regime. By modeling mantle convection in a spherical annulus, we analyze the impact of grain size evolution (GSE) on the global tectonic style. We find that grain size reduction suppresses episodic behavior and facilitates surface mobility over a range of lithospheric yield stresses, but GSE has no discernable effect on the transition to stagnant-lid tectonics. Moreover, increased grain growth does not

Email address: a.cordoba@ucl.ac.uk (Antonio Manjón-Cabeza Córdoba)

result in higher episodicity either. GSE, together with composite rheology, modify the diagnostics within one tectonic regime. These findings support the importance of grain size evolution for stabilizing mobile-lid tectonics, but also cast doubt on the potential of damage to explain mobile-lid tectonics up to laboratory-inferred strengths.

Keywords:
Grain Size Evolution, Convection Models, Planetary Convection, Tectonic Regime

1. Introduction

The thermal evolution of a rocky planet is determined by its tectonic mode, which asserts a first-order control on that planet history (e.g. Crameri et al., 2019; Rolf et al., 2022). This tectonic mode or regime is important for core and magnetic field evolution, magmatism and volatiles circulation, atmosphere, sea level, and ultimately habitability (Foley, 2015). The Earth features a tectonic mode, plate tectonics (more generally mobile-lid), characterized by constant creation of lithosphere and its recycling into the mantle in narrow plate boundaries that bear most of the surface deformation. This regime, however, is absent on any other planet with a known tectonic regime. Instead, other bodies like the Moon, Mercury or Mars present a stagnant-lid regime, characterized by a continuous and immobile upper thermal boundary layer (lithosphere) with much less efficient recycling of material into the convecting mantle (e.g. Stern et al., 2018; Tosi and Padovan, 2021). Venus may have a different, yet-to-be-defined regime between mobile lid and stagnant lid (Byrne et al., 2021; Rolf et al., 2022; Tian et al., 2023).

To date, the exact factors conditioning the tectonic regime of a rocky planet have not been unequivocally determined. In global-scale geodynamic models, the tectonic regime is mainly a result of a yield stress, which controls the strength of the lithosphere. The tectonic limits defined by this yield stress can further vary depending on other parameters that are not always present in all geodynamic models (Lourenço and Rozel, 2023). This yield stress is, however, a simplification of the physical phenomena taking place in the deforming lithosphere (Karato, 2010; Warren and Hansen, 2023). Moreover, the values required to reproduce plate tectonics on Earth-like models are lower than any laboratory measurement of pristine rock (Brace and Kohlstedt, 1980; Alisic et al., 2010; Hirth and Kohlstedt, 2015).

In nature, the lithospheric strength is most likely a combination of thermal and compositional effects, and of processes operating at different spatial-temporal scales. In particular, rheology is known to play a key role by coupling the aforementioned processes and ultimately defining the effective yield stress of the lithosphere (e.g. Bercovici et al., 2015; Arnould et al., 2023). One parameter explored in calculations simulating realistic mantle deformation is the mineral grain size, known to directly affect the rheology of the mantle and the strength of the lithosphere (Platt and Behr, 2011; Vauchez et al., 2012). Small grain sizes in deformed shear zones point to a direct relation between weakening and grain reduction (Warren and Hirth, 2006; Newman and Drury, 2010). Likewise, experimental and theoretical work suggests a critical importance of grain size in several deformation mechanisms (e.g., diffusion creep or grain boundary sliding; Karato and Wu, 1993; Hansen et al., 2012; Kohlstedt and Hansen, 2015).

This corpus of evidence begets the question whether grain size and its dynamic evolution, driven by deformation-assisted reduction and subsequent growth by thermal healing, are critical for the development of the tectonic mode of a planet (Bercovici and Ricard, 2014). On the one hand, grain reduction should reduce viscosity and help to decrease the strength of previously deformed lithosphere, promoting subduction and ridge creation. Effectively, this reduction would increase the maximum yield stress that could be used by tectonic models to recreate the mobile-lid regime (Bercovici and Ricard, 2012), hence bringing these yield stress values closer to laboratory experiments. On the other hand, grain growth counteracts the previous effect and promotes increasing viscosities in regions of the mantle dominated by diffusion creep (e.g., the lower mantle; Solomatov, 1996).

Due to the apparent importance of grain size evolution (GSE), some work has focused on exploring how GSE and its governing parameters influence the tectonic mode. Earlier models used simplified approximations to mantle convection and GSE evolution to explain differences between the different bodies of the solar system (e.g., Solomatov, 2001; Landuyt and Bercovici, 2009). Only recently have modelling studies explicitly considered GSE and mantle convection in a fully self-consistent manner, using state-of-the-art descriptions of GSE (Austin and Evans, 2007; Rozel et al., 2011). For example, Dannberg et al. (2017) gave an extensive description of the effects of GSE on mantle dynamics, but focused specifically on subduction and plume upwelling, and very constrained GSE parameters. More recently, Schierjott et al. (2020) performed a systematic parameter search, but focused on the preservation of thermochemical piles rather than on the GSE effects on the tectonic regime. Foley and Rizo (2017) did focus on the mobile-lid regime, but neglected dislocation creep, which could lead to significant differences at depths of the lithosphere-asthenosphere boundary (Arnould et al., 2023). In the most recent years, the focus of GSE-dependent models has shifted to understanding very specific systems (e.g., Paul et al., 2024), but in order to represent specific planets (e.g., the Earth, Venus), these models include additional specific phenomena (such as melting, phase transitions...), that tend to obscure the effects of grain size evolution.

Whether owing to their simplicity or complexity, none of these works describes how different amounts of grain growth and grain reduction affect the tectonic regimes in a self-consistent manner. To date, how different diagnostic characteristics of these regimes (e.g., internal temperature or surface velocity) vary within one regime, or among them, depending on GSE parameters, is still unknown for a system with composite rheology and varying GSE parameters. This sort of description is essential to understand the differences between solar system bodies, but also to understand how more specific (Earth-like) models may differ from generic cases. Furthermore, this description may answer the question of why some studies have struggled to find the mobile-lid regime (Rozel, 2012; Schierjott et al., 2020), even when the null hypothesis is usually that GSE consideration should help geodynamic models broaden the interval of yield stress values for which mobile lid occurs (Bercovici and Ricard, 2014).

In this article, we focus on the changes that the different tectonic modes undergo when systematically changing GSE parameters that affect the grain growth/reduction linearly. We run 2D whole-mantle numerical experiments with composite rheology coupled with grain-size evolution and evaluate their main features. In addition, we vary the yield stress of our models under given sets of GSE parameters to understand how grain reduction and growth affect the feasibility of plate tectonics (mobile lid) and other tectonic regimes.

2. Methods

2.1. Model setting and numerical approach

We run numerical experiments using the code StagYY (Tackley, 2008) with a nominal Rayleigh number of Ra=10^7 (defined at the reference conditions listed in table 1). The code solves the incompressible Stokes equations in annulus geometry under the extended Boussinesq approximation incorporating internal, adiabatic and shear heating (Christensen and Yuen, 1985). We employ a viscoplastic rheology approximating two coexisting creep mechanisms of deformation - diffusion creep and dislocation creep - with an Arrhenius law dependent on pressure (P) and temperature (T):

$$\eta_{mech} = \eta_0 \left(\frac{\sigma}{\sigma_0}\right)^{1-n} \left(\frac{D}{D_0}\right)^{m} \mathrm{e}^{\frac{E_{mech}+PV_{mech}}{RT}} \qquad (1)$$

where η, σ and D are the viscosity, the stress and the grain size, respectively, with the subscript '0' referring to their reference value. E and V are the activation energy and volume, and the subscript *mech* corresponds to the different mechanisms of deformation (dislocation or diffusion). The exponent n is 3.5 for dislocation creep and 1 for diffusion creep; m is 0 in dislocation creep and 2 in diffusion creep. The choice of m=2 (Nabarro-Herring Creep dominates over Coble creep) is aligned with some of the literature (e.g., Jain et al., 2019), but other works favor a value of $m = 3$ (Coble Creep dominates;

Hirth and Kohlstedt, 2003). It is far from the objective of this work to solve an issue of current discussion in the field of mineral physics (e.g., Jain et al., 2018). From the numerical perspective, an exponent of 2 is easier to solve and allows us to study a wider range of parameters. Faced with the choice of a possible underestimation (m=2) or overestimation (m=3) of the effect of grain size in the viscosity, we choose the former and interpret our results accordingly.

In addition to these two creep mechanisms, we consider plastic yielding: $\eta_y = \sigma_y/2\,\dot{\varepsilon}_{II}$ (e.g., Trompert and Hansen, 1998), where $\dot{\varepsilon}_{II}$ is the second invariant of the strain rate tensor and σ_y is the depth-dependent yield stress increasing from a surface value $\sigma_{y,0}$ downwards with a rate σ'_y. All three viscosity mechanisms coexist, with the effective viscosity given as $\eta = 1/(1/\eta_{disl} + 1/\eta_{diff} + 1/\eta_y)$. Table 1 shows all parameters used in this work, whose values (unless explicitly mentioned) are nondimensional throughout the text.

To model grain-size evolution, we follow the thermodynamically self-consistent approximation of Rozel et al. (2011):

$$\frac{dD}{dt} = \frac{k\,\mathrm{e}^{\frac{-E^*}{RT}}}{qD^{q-1}} - c\,D^2\,f_G\,\sigma\colon\dot{\varepsilon}_{disl+y} \tag{2}$$

where k is an empirical prefactor and E^* the activation energy for grain growth. c is a semi-empirical constant of grain reduction (for a full description see Rozel et al., 2011), and f_G describes the fraction of the dissipation due to dislocation creep and yielding ($\sigma\colon\dot{\varepsilon}_{disl+y}$) which causes grain reduction (diffusion creep does not contribute to grain reduction). In our models, f_G may remain constant throughout the mantle or be dependent on tempera-

Table 1: List of parameters used in this work. Intervals show values explored. The constant c is described in full in Rozel et al. (2011). All values are dimensionalized taking as reference the Rayleigh number $Ra = \frac{\Delta T\ \alpha\ \rho_0\ g\ Z^3}{\eta_0\ \kappa} = 10^7$; and the Dissipation number $Di = \frac{\alpha\ gZ}{C_P} = 0.4$. Note that any other combination of parameters for which $Ra = 10^7$ and $Di = 0.4$ is consistent with our calculations.

Parameter	Abbreviation	Non-dimensional value	Dimensional value	Units
Temperature drop	ΔT	1	2500	K
Reference density	ρ_0	1	3300	kg m^3
Mantle thickness	Z	1	2.89×10^6	m
Thermal expansivity	α	1	5×10^{-5}	K^{-1}
Thermal diffusivity	κ	1	10^{-6}	m^2 s^{-1}
Gravitational acceleration	g	1	9.81	m s^{-2}
Reference viscosity	η_0	1	9.77×10^{21}	Pa s
Heat capacity	C_P	1	3.54×10^3	J K^{-1} kg^{-1}
Reference stress	σ_0	2000	2.34×10^6	Pa
Reference grain size	D_0	5×10^{-9}	1.45×10^{-2}	m
A. Energy (diffusion creep)	E_{diff}	6	1.25×10^5	J mol^{-1}
A. Energy (dislocation c.)	E_{disl}	11	2.29×10^5	J mol^{-1}
A. Volume (diffusion creep)	V_{diff}	5	1.11×10^{-6}	m^3 mol^{-1}
A. Volume (dislocation c.)	V_{disl}	35	7.78×10^{-6}	m^3 mol^{-1}
Yield stress (surface)	$\sigma_{y,0}$	10^3 - 10^6	(1.17-1170) $\times10^6$	Pa
Yield stress (slope)	σ'_y	0.14	4.53×10^3	Pa m^{-1}
Grain growth constant	k	5×10^{-27}-5×10^{-25}	4.2×10^4-4.2×10^6	μm^4 s^{-1}
A. Energy (grain growth)	$E*$	8	1.66×10^5	J mol^{-1}
Grain reduction constant	c	1.651×10^9	0.488	Pa^{-1} m^{-1}
G. red. work fraction	f_G	10^{-7}-10^{-2}	-	-
Radiogenic heating	H	30	3.18×10^{-11}	W kg^{-1}

ture as described in Schierjott et al. (2020): $f_G = f_{surf}(f_{cmb}/f_{surf})^{T/T_{cmb}}$, where f_{surf} is the value at the top boundary (T=T_{surf}=0.00) and f_{cmb} is the value at the bottom boundary (T=T_{cmb}=1.49). Theoretical estimations of the exponent q valid for a polymineralic rock range from 3 to 5 depending on the growth mechanism (note that a value of 2 is valid for a suspension, but this will not be the case for mantle rocks; Wagner, 1961; Ardell, 1972; Solomatov et al., 2002); we choose a value of 4 as an intermediate value, but other values are also common in the literature (e.g., Dannberg et al., 2017; Paul et al., 2024).

We resolve the model domain with 128 grid nodes in the radial direction and 1536 nodes in the angular direction. Vertical grid refinement is applied at the top and bottom boundary layers. This results in a maximum vertical resolution of 0.00401 at the top boundary layer (dimensionalized 11.6 km), 0.005968 (17.3 km) at the bottom boundary layer, and minimum resolution of 0.010566 (30.54 km). We carry the grain size information on 11×10^6 tracers (56 per cell on average). The top and bottom boundaries are free-slip with constant temperature. The bottom temperature of $T_{cmb} = 1.49$ accounts for both, the adiabatic and superadiabatic temperature increase across the mantle assuming a dissipation number of $Di = 0.4$.

The mantle is internally heated with a constant nondimensional rate of 30. Dimensionalized (Table 1), this value yields a radiogenic heat production higher than estimated for the Earth (Turcotte and Schubert, 2014), but this is a common adjustment for steady state models trying to simulate a non-steady state (cooling) Earth (Korenaga, 2017). The initial thermal field was obtained by running a preliminary model without GSE until a spontaneous subduction zone develops. This initial state is rather arbitrary but allows for a direct comparison between models that may be affected by hysteresis (Weller and Lenardic, 2012; Bercovici and Ricard, 2016). All models are run until statistical steady state is reached; all diagnostics and properties presented below are averaged over the time in steady state only. Supplementary Table S1 shows a list with all the model runs and the properties that are changed from model to model.

2.2. Diagnostics

To characterize the dynamic regime of the presented models, we use the surface mobility (M) as defined in Tackley (2000) $M = v_{hsurf,rms}/v_{rms}$, that is: the root mean square of the horizontal surface velocity divided by the root mean square of the internal velocity. When averaging this parameter over time, its value may not discriminate between the episodic and mobile regime (as they both can have similar averages but different standard deviations). To further discriminate between regimes, we introduce an additional parameter called 'tranquillity' ($0 \leq \tau_M \leq 1$), defined as the proportion of steady-state run-time during which $M \leq M_{crit}$. This diagnostic quantifies better the temporal fluctuations in surface velocity: a value of τ_M=1 signals the stagnant-lid regime, while values significantly lower than 1 and closer to 0 correspond to the mobile-lid regime.

We chose a M_{crit} of 0.9 which is meaningful for our models (see Figure 2), but any value chosen would be arbitrary. To measure the uncertainty of τ_M, we also show an error bar calculated considering a M_{crit} of 0.85 (lower limit) and 0.95 (upper limit) in Figures 4c,f and 7. Note however that in this case the errors are correlated among them, that is, it is not correct to compare the error for the threshold of 0.85 with the error for the threshold of 0.95 (comparing upper with lower limits is not strictly correct).

In addition to M and τ_M, we also report global averages such as grain size or temperature (T). We also calculate surface properties like surface velocity (v_{hsurf}) or subduction zones number ($Subduction\ \#$), calculated as number of convergent peaks in surface velocity. All averages are both spatial (across the whole model) and temporal (across all of the steady state duration). As specified before, surface velocity is calculated as $v_{hsurf,rms}$. All these properties are shown with the corresponding (temporal) standard deviation as an error.

Furthermore, we show two additional properties: minimum viscosity (as $\log(\eta_{min})$) and thermal boundary layer thickness(as d_{TBL}), for both the top and bottom boundary layers. The minimum viscosity corresponds to that of the asthenosphere (in our models, due to grain growth, the viscosity of the asthenosphere is lower than that of the core-mantle boundary, see below). Instead of the standard deviation for a time average, we show the difference between the maximum average (in angular direction) for the minimum viscosity and the minimum average (in angular direction) of the maximum viscosity at that depth (corresponding to dashed green lines in Figure 2b). We found these values more informative than the standard deviation in time (which was extremely small for many models).

The thermal boundary layer thickness (d_{TBL}) corresponds to the depth of minimum viscosity (upper TBL thickness) and the depth of maximum viscosity excluding the top boundary layer (lower TBL thickness, see Figure 2). While the thermal boundary layer can be defined following different approaches, we found the viscosity minima and maxima to be good dynamic proxies. For similar reasons as for the viscosity, the error of the d_{TBL} data points does not correspond to the standard deviation; instead, it corresponds to the grid resolution at that depth (as the standard deviation was smaller than the grid resolution).

3. Results

3.1. Reference case

Figures 1 and 2 show the results for the reference case using k=5×10^{-26} and f_G=1×10^{-6} (independent of temperature), with a surface yield stress of $\sigma_{y,0}$=5×10^3. Field snapshots show association between low-temperature regions and small-grain-size regions (Figure 1a-c). This is expected due to the strong temperature dependence of the grain growth term (Eq. 2). In addition, yielding strongly reduces grain size at shallow areas with high stress. Areas of low temperature and small grain size also present high viscosities, which suggests that the viscosity is still mainly temperature-dominated. Areas with significant dislocation creep (Figure 1d) are almost exclusive to the uppermost mantle and always associated with subduction zones and mid-ocean ridges. This association creates noticeably lateral (angular) viscosity differences in the asthenosphere. These differences are markedly time-dependent (see supplementary video SV1).

These characteristics are confirmed by the radial profiles (Figure 2a-c and Figure 3). A notable exception is the asthenophere, where small grain sizes can occur despite high temperatures (and therefore low viscosity values) due to dislocation creep and dynamic recrystallization, and lateral contrasts are

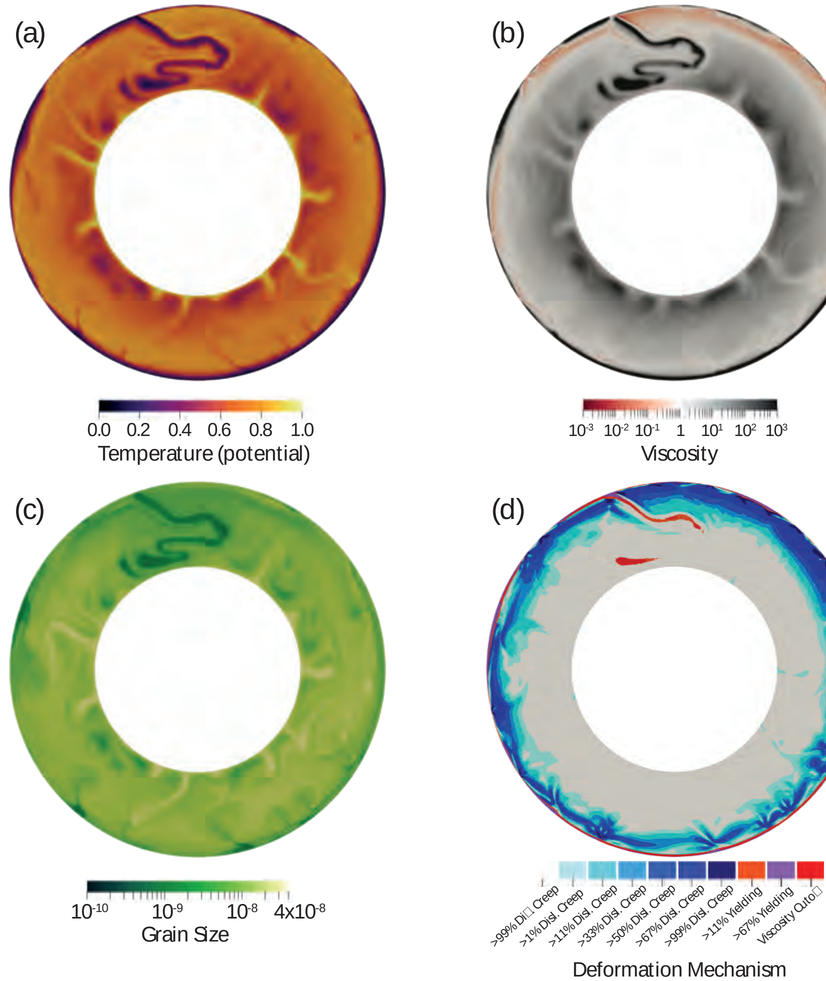

Figure 1: Representative snapshots of the reference case. (a) Potential temperature (adiabatic gradient removed). (b) Viscosity (log scale), with an upper saturation at 10^3 (maximum is 10^4), (c) grain size, (d) deformation mechanism.

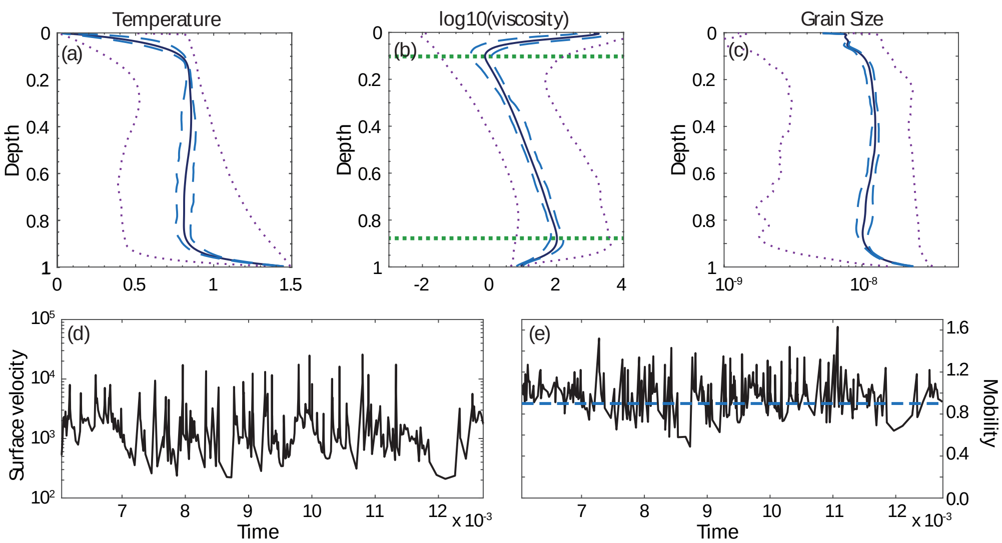

Figure 2: Main convective characteristics of the reference case. (a) Total temperature radial profile (including adiabatic gradient), (b) viscosity radial profile, the dashed green line corresponds to the depths of minimum/maximum viscosity, which are used for calculations pertaining the TBL (see text), (c) grain size radial profile. For panels a-c, blue dashed lines represent the temporal variation in the average values, while the dotted purple lines represent the average minimum and maximum radial profiles. (d) Average horizontal surface velocity (see text for definition), (e) surface mobility, the 0.9 limit to separate "subduction" time and 'tranquil' time is indicated by the horizontal blue dashed line. In this case, the tranquillity is τ_M=0.26.

very stark, as mentioned above (Figure 1b,d). In the lower mantle, viscosity contrasts are considerably smaller far from subduction zones (i.e., $\leq 10^2$), with little difference between high and low temperature regions (Figure 1b). As in Arnould et al. (2023), plumes show deformation mainly at their 'flanks', which in our case causes plume conduit 'cores' to feature the greatest grain sizes and relatively high viscosity. The minimum viscosity corresponds to the asthenosphere and not the core-mantle boundary, as would be common in models without GSE (Supplementary Figure S1).

The reference model shows a mobility of M=0.94 $\pm$0.20 and a tranquillity of τ_M=$0.26^{+0.10}_{-0.10}$ (the difference in notation is due to the fact that, in the tranquillity case, the uncertainties may not be symmetric: the equivalence of the absolute value of the lower and upper error is a coincidence). These values make the reference case representative of the mobile-lid regime, which is also indicated by the presence of at least one active subduction zone throughout most of the time evolution. Still, a pronounced time dependence is observed (Figure 2d,e), which arises from the cessation of mature subduction zones and the onset of new ones.

3.2. Grain size evolution parameters systematics

We explore the effect of GSE on mobile-lid convection by varying the parameters f_G and k. These parameters, respectively, affect the grain reduction and grain growth terms in a linear fashion. Changing q or E^* would have a stronger albeit nonlinear effect, but in chaotic systems (i.e. high Ra number) non-linearity may obscure the interpretation of the results. We test different uniform values of f_G (i.e., f_{surf}=f_{cmb}=10^{-7}-10^{-4}) and k (k=5×10^{-27}-5×10^{-25}). In addition, we investigate the temperature dependence of f_G by

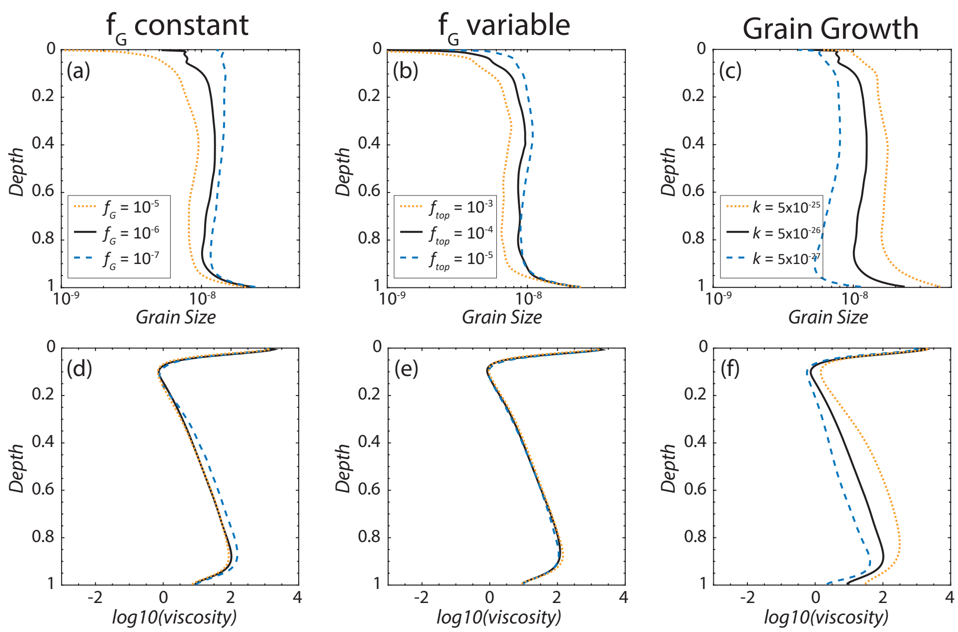

Figure 3: Average radial profiles of grain size and viscosity from cases discussed in the main text. (a-c) Grain size profiles showing that the greatest effect on the grain size in the asthenosphere depends on f_G, while for the lower mantle variation of viscosity and grain size depends more strongly on the grain growth parameter k (d-f). The self-regulatory character of GSE, giving similar viscosity profiles for different values of grain reduction (e.g., panels d and e) has been pointed out elsewhere (e.g. Schierjott et al., 2020)

fixing f_{cmb} (=10^{-7}) while varying f_{surf} (=10^{-5}-10^{-2}).

Figure 3 shows the change radial profiles of grain size and viscosity. A noticeable characteristic is the extremely small change in viscosity values for different f_G, whether constant or variable. This is easily explained by the dependence of grain reduction on dissipation (and therefore stress). Due to the piezometric qualities of grain size (Austin and Evans, 2007) and the composite rheology of our models, viscosity will tend to regulate itself via more efficient cooling (i.e., via the temperature-dependence of the viscosity, eq. 1) and grain size reduction. This self-regulating behavior, also seen in other works (Austin and Evans, 2007; Schierjott et al., 2020; Okamoto and Hiraga, 2024), is further addressed in the discussion section. Regardless, this behavior is missing from the profiles of changing k (figure 3c,f), where grain size changes strongly across the whole mantle, and viscosity changes are systematic and more important than in the cases of changing f_G.

Varying both f_G and k results in differences in the average grain size as expected (Figure 4a,d). k has a starker effect on the average grain size, but this is likely due to the effect of f_G being restricted to areas of the model under predominant dislocation creep or yielding, which are mostly limited to the upper mantle and lithosphere. For the cases with temperature-dependent f_G, grain reduction is even more restricted to low temperature areas. Consequently, the trend in average grain size is gentler than in the case with constant f_G. However, while decreasing grain size via increasing grain reduction effectively weakens the lithosphere, enhancing subduction (Figure 5a,d), and therefore decreases mantle temperature, increasing grain size via increasing k also results in lower temperatures. Hence, our models

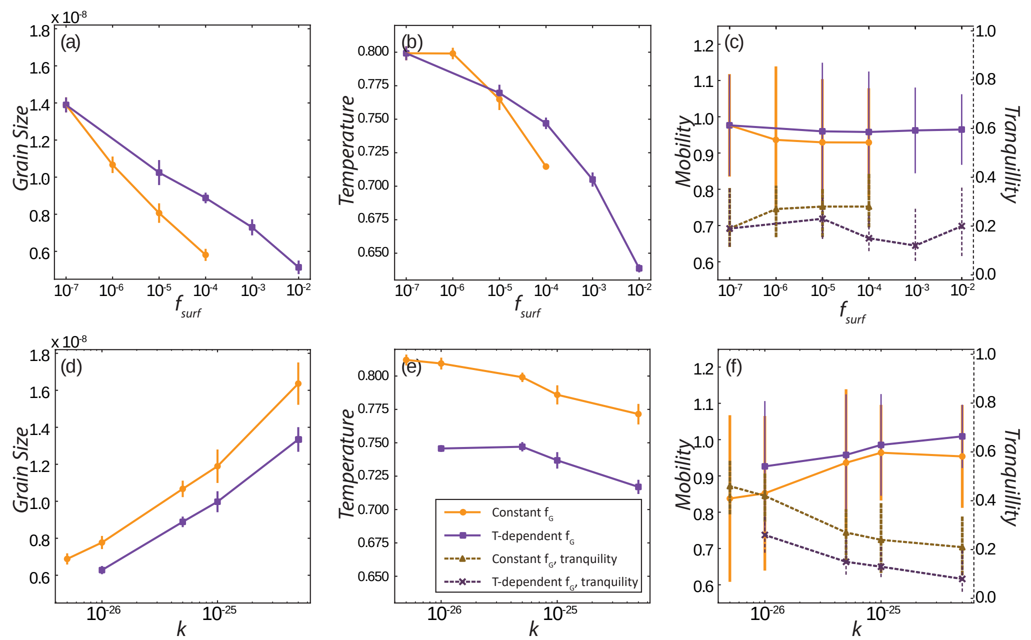

Figure 4: Diagrams showing the variation of average (depth and time) grain size, internal temperature mobility/tranquillity with different GSE parameters. In panels a-c, the line for constant f_G has equal f_{surf} than f_{cmb}. In panels d-f, the line for variable f_G has a fixed f_{surf} value of 10^{-4}. For further details see text.

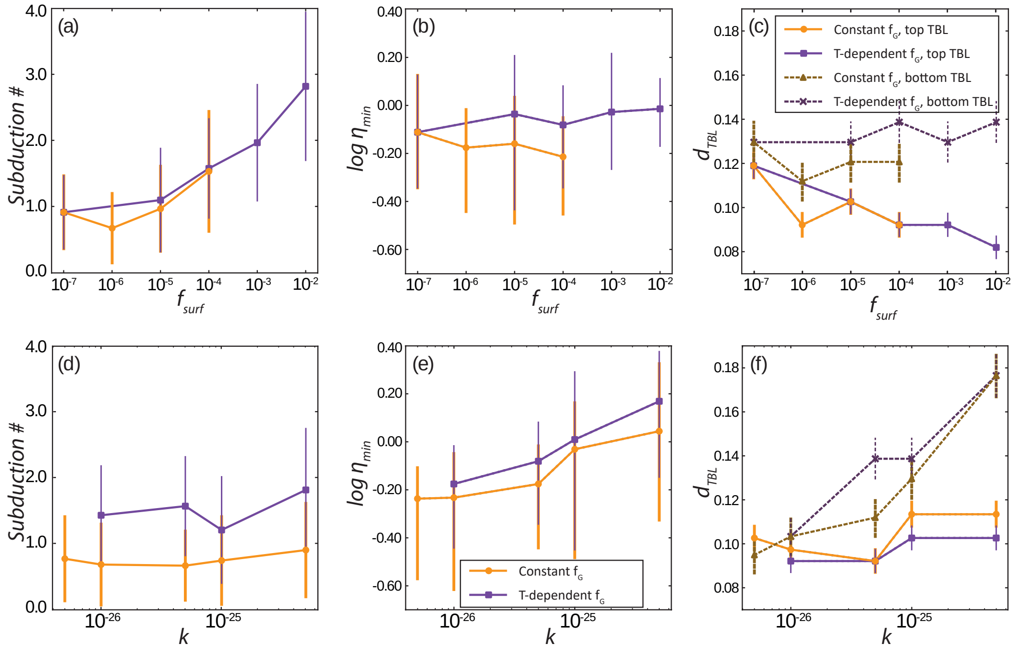

Figure 5: Diagram showing secondary diagnostics variation with grain size parameters. Colors and symbols as in Figure 4 except for panels (c) and (d) which track the upper and lower thermal boundary layer thickness as defined in the text.

show opposite correlations (positive vs. negative) between grain size and temperature depending on the varied parameters, f_G or k (Figure 4b,e). This is apparently counter-intuitive and at odds with previous interpretations of healing in the lithosphere (Fuchs and Becker, 2022; Mulyukova and Bercovici, 2023).

M decreases slightly with increasing grain reduction, and increases with increasing grain growth (Figure 4c,f). τ_M decreases with increasing mobility for most cases. However, in the case of variable f_G (purple line in Figure 4c), the minimum tranquillity is obtained at $f_{surf} = 10^{-3}$. Partly, the increase in mobility with higher grain growth could be explained by the increase in viscosity in the lower mantle and the corresponding decrease in flow velocities (see also Figure 3). However, the opposite correlation between grain size and temperature mentioned above suggests an influence of the grain growth parameter k on the subduction efficiency. Cases with high f_G do feature more subduction zones (Figure 5a, see also Fuchs and Becker, 2019, 2022) and more efficient cooling, but these slabs eventually become very weak and break off (hence the decrease of mobility with higher f_G). Supplementary video SV1 shows an example of this sort of tectonics.

Additional diagnostics are shown in Figure 5. As mentioned above, the number of subduction zones increases when increasing grain reduction (Figure 5a). This is expected from previous work and signals the relation between damage and subduction zone creation (Bercovici and Ricard, 2014; Fuchs and Becker, 2019). Contrary to this, we do not find an evident relation between increasing grain growth and *subduction #* (Figure 5d), meaning that if there is a relation between k and subduction efficiency, as suggested above, it should be in the persistence of subduction zones. The viscosity of the asthenosphere seems fairly constant for models with different f_G, although there may be a small decrease when f_G is independent of temperature (Figure 5b, orange line). On the contrary, increasing grain growth does change the minimum viscosity (Figure 5e), albeit slightly, which remains puzzling because the same models have an increasing mobility and decreasing tranquillity. Finally, the relation between thermal boundary thickness seems a bit more straightforward, with the upper d_{TBL} quasi-independent of grain growth but considerably affected by increasing f_G (Figure 5c,f); meanwhile,

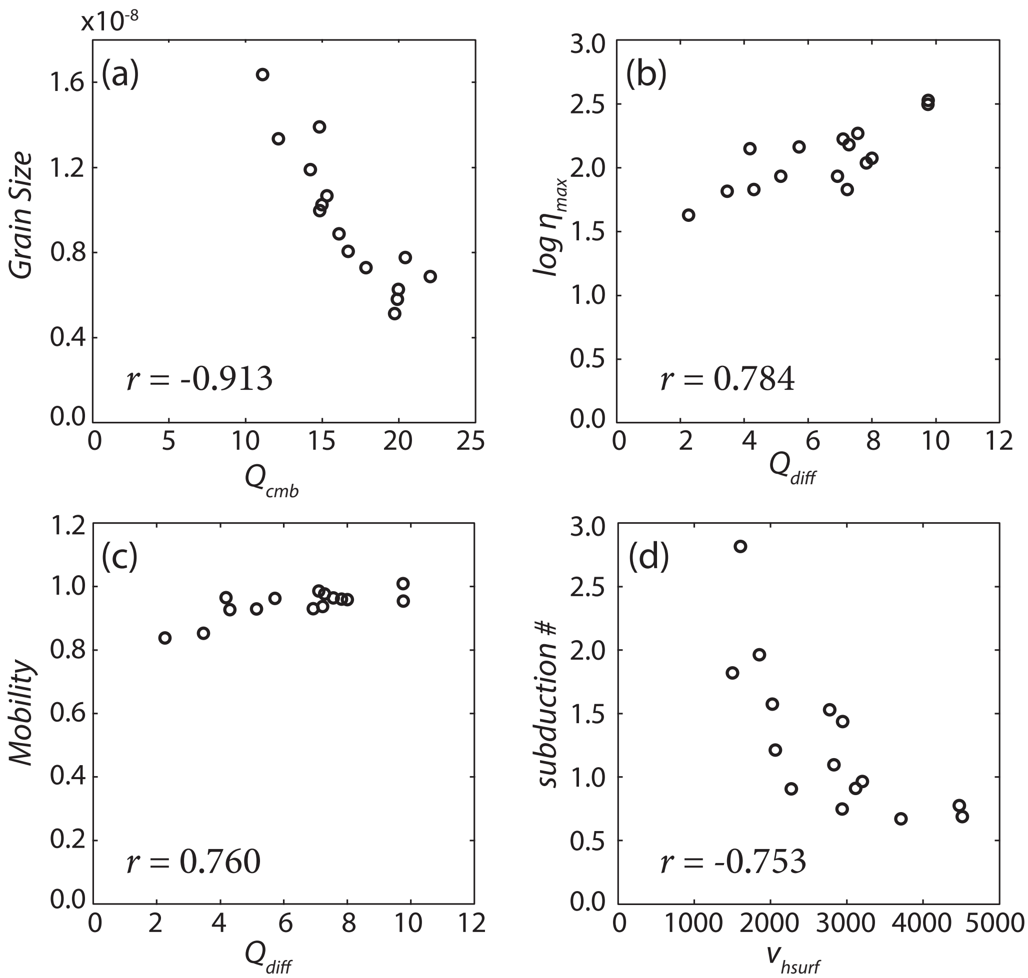

Figure 6: Correlations between model diagnostics. All datapoints correspond to models shown in Figures 4 and 5. Note that the Pearson correlation coefficient r refers to the linear relation of the normalized data. For panel (d), if *subduction #* is transformed to $1/subduction$ #, $r = 0.827$. Please mind that correlation does not necessarily imply causation. For a full description of axes see text.

the bottom d_{TBL} shows the opposite, with a marked increase when increasing k but near independence of f_G due to the absence of dislocation creep near the core-mantle boundary.

The internal temperature of steady state convection models is a function of the heat flow at the base and the surface, the internal heating, d_{TBL} and recycling efficiency. To better understand the puzzling relations between GSE parameters, tectonic activity and internal temperature, we plot diagnostic vs. diagnostic diagrams in Figure 6. The strongest correlation that we find with the bottom heat flux (Q_{cmb}) is the average grain size (Figure 6a): the greater the average grain size, the lower the heat flow. This is consistent with Figure 5f, which finds a strong k-dependence of the bottom d_{TBL}. Since our models are internally heated, Q_{cmb} does not need to be equal to Q_{surf} (surface heat flow): we plot Q_{surf}-Q_{cmb} as Q_{diff} in Figure 6b,c. The smaller the number the lower the contribution of internal heat to Q_{surf}, and therefore the greater efficiency of top-to-bottom convection. We find that the maximum viscosity (lower green line in Figure 2b) correlates the strongest with this parameter (based on the Pearson correlation coefficient r for normalized data), with high lower mantle viscosities corresponding to high Q_{diff}.

Tectonic efficiency is expected to contribute to Q_{diff} as well. M and Q_{diff} also show a high r (Figure 6c). However, the slightly positive slope shown is the opposite that we would expect, assuming that a greater Mobility should contribute to more efficient cooling, lower internal temperatures and lower Q_{diff}. To fully understand these processes, we plot v_{hsurf} vs. *subduction #* (Figure 6d). An interesting picture emerges where cases with the highest subduction number (i.e., cases with the highest f_{surf}; Figure 5a) feature the lowest horizontal surface velocity. This implies that cases that are cooling very efficiently (i.e., small Q_{diff}, lowest temperatures in Figure 4b,e) do not need to show high Mobility. Instead, high plate velocities correspond with fewer *subduction #*.

3.3. Yield stress systematics

We also varied the surface yield stress ($\sigma_{y,0}$) for different sets of GSE parameters (k and f_G). Figure 7 shows the change in tranquillity based on the yield stress of those models. The transition between episodic and mobile-lid is slightly arbitrary in terms of both, mobility and tranquillity, but the slope of tranquillity provides a reproducible way to distinguish between the regimes. For example, for the stagnant-lid regime the slope is necessarily 0, and for continuous mobile-lid this slope is similarly very small, yet it is very steep for the episodic regime. With this definition, the transition between mobile and episodic can happen at different tranquillities for different GSE properties (Figure 7). This difference reflects the different strengths and continuities of the subduction slabs, as well as different subduction speeds. It is also worth noting that, in this work, the episodic regime is not equivalent to the catastrophic overturns in other works (e.g., Uppalapati et al., 2020): in our models, episodic cases feature events that do not recycle the whole lithosphere. Moreover, the phases between episodes with subduction are similar to the “ridge only” cases of Rozel et al. (2015).

For the reference set (black lines in figure 7), mobile cases present a near constant tranquillity around a value of 0.25, while we deem episodic the cases that form the strong slope between mobile cases ($\sigma_{y,0} \leq 10^4$) and stagnant lid ($\sigma_{y,0} \geq 3{\times}10^5$). The reference profile shows the transition from episodic to stagnant lid (τ_M=1) occurring between $\sigma_{y,0}$=10^5 and $\sigma_{y,0}$=3×10^5. This transition is the same for the case with stronger grain reduction (f_G=10^{-4}-10^{-7}; Figure 7a), and faster grain growth ($k = 5\times10^{-25}$; Figure 7b).

The transition between mobile-lid and episodic-lid regimes for different GSE properties does feature differences from the reference case, with the cases with higher grain reduction (f_{surf}=10^{-4}) and higher grain growth (k=5×10^{-25}, Figure 7) showing mobile lid at higher $\sigma_{y,0}$. Moreover, cases with very high yield stress are still very 'mobile' (low tranquillity) for the cases with temperature-dependent grain reduction (Figure 7). With respect to the constant f_G cases, these cases may show greater average grain size and greater average viscosity for the same yield stress (Figure 4), but they show lower 'tranquillity', showcasing the importance of the temperature effect of f_G for the stability of plates. Moreover, the transition between stagnant lid and mobile lid occurs over a smaller range of yield stresses (as a result of the "reduced" episodic regime).

The trend with constant grain size (Figure 7) shows no clear difference from GSE models as far as the transition yield stress between episodic-lid and stagnant-lid is concerned. Because we chose a reference grain size, D_0=10^{-8}, intentionally to be similar to the average grain size obtained for the reference case (supplementary Figure S1), values of tranquillity are similar to the case with low grain growth and grain reduction (reference case), but very different from the other cases (even if for those cases the grain size is similar, as is the case of increased grain growth). However, similar τ_M does not necessarily imply similarities in other properties (for a further comparison between variable and constant grain size, see supplementary figure S1).

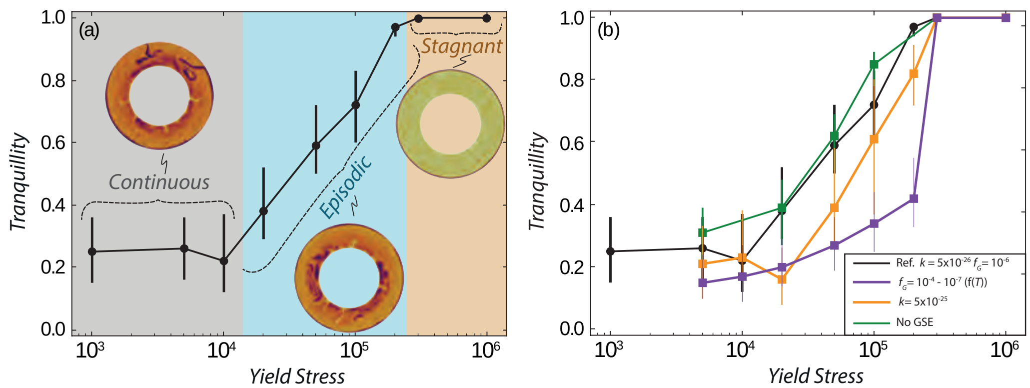

Figure 7: tranquillity (τ_M) vs. yield stress diagram. Each line reflects the transition from mobile lid to stagnant lid for different GS parameters. (a) Reference case with the limits of the tectonic regimes highlighted by color. The initial near-constant tranquillity at low yield stresses reflects the mobile lid. The slope at intermediate stresses corresponds to episodic cases. The flat section at $\tau_M = 1$ represents the stagnant lid cases. (b) Cases with different GSE properties. While the transition between episodic and stagnant tectonics does not change, the tranquillity for the episodic regime differs greatly among cases.

4. Discussion

4.1. Effect of GSE on global tectonics

In this study, we investigated how grain-size evolution (GSE) impacts the tectonic regimes arising from mantle convection. Several authors predicted that GSE, particularly when strong grain reduction is present, would favor a higher critical yield stress for the transition between stagnant lid and episodic or mobile-lid regimes (Rozel, 2012; Bercovici and Ricard, 2014). Our models do not show any evident change of yield stress for the transition between the episodic and stagnant regimes (Figure 7). Instead, the critical yield stress remains similar regardless of the GSE parameters, although the transition between stagnant and episodic may be more or less abrupt in terms of mobility jump (or tranquillity) with different GSE parameters.

Our models do suggest, however, that increased grain reduction may favor a continuous mobile-lid regime, as opposed to an episodic regime, hinting at the role of inheritance to stabilize subduction zones (e.g. Fuchs and Becker, 2019). This may reduce the feasibility of the episodic regime, which is also in contrast with previous work that found a large transition between mobile-lid regime and stagnant-lid regime (Foley and Bercovici, 2014); the main difference being that we include dislocation creep and a yield stress in our models. Particularly, the trend of temperature-dependent grain reduction (purple line in Figures 4, 7) shows low tranquillity for any model not in stagnant lid (Figure 7b), suggesting a very narrow transition between mobile and stagnant lids.

Regarding grain growth, an increased value of k does not preclude the persistence of subduction zones (Bercovici and Ricard, 2014). The higher end of the grain growth k used in our models resembles realistic olivine grain growth laws (Table 1; Schierjott et al., 2020), but more importantly, we explore several orders of magnitude of change with little effect in the tectonic regime limits. These results suggest that healing plays a minor role in the definition of the tectonic regime (i.e., its limits), at least within the assumptions of our models (i.e., as grain growth remains temperature-dependent with an activation energy of the same order of magnitude as diffusion and/or dislocation creep; Okamoto and Hiraga, 2024). This is consistent with the findings of Arnould et al. (2023), who found that dislocation creep fosters decoupling of the lithosphere and asthenosphere, decreasing the effect that asthenospheric stresses have on subduction zone creation. Healing will be further limited in systems considering pinning (Bercovici and Ricard, 2012), which, for simplicity, is not explicitly included in this work.

Certainly, while transition between regimes may depend only weakly on GSE parameters, this does not mean that grain size does not affect properties of the convective system within one regime. Indeed, Figure 4 shows that within the mobile lid regime, properties such as internal temperature can be highly dependent on grain growth and reduction. Changing grain growth and grain reduction parameters modulates the average grain size of a planet as expected. Concerning global average internal temperature, however, the relation is less straightforward. Due to the decreased temperature with increasing both k and f_G there is no univocal relation between average grain size and internal temperature (or, in steady-state models, cooling efficiency).

While correlation does not imply causation, Figures 4, 5 and 6 allow us to deduct the effects of k and f_G within the mobile regime. The grain growth prefactor k has a marked effect on the thickness of the bottom d_{TBL} (Figure 5f). Bottom heat flow (Q_{cmb}) is therefore hampered by increasing grain growth (Figure 6). The lower internal temperature of high grain growth models is likely a consequence of the lower heat flow from the core. Compared with models of high f_G, these models also feature an inefficient convective heat transfer (high Q_{diff}, Figure 6b), partly because the Ra decreases with increasing viscosity (Figure 3d,f), and a higher contribution of internal heating to surface heat flow. Meanwhile high f_G models should feature a higher heat flow from the bottom, but an increase in *subduction* # (Figure 5a) more than compensates for this heat flow, causing also a decrease in global internal temperature.

As mentioned in section 3, healing does not have a strong effect in our models, likely due to the activation energy in Eq. 2. Moreover, it is likely that healing would be of secondary importance in our models even with lower E^*. Cases with high k feature high mobility and low tranquility. Not only is this effect due to an internal sluggish convection owed to increased η_{max} (lower v_{rms}), but actually models with a lower number of subduction zones feature higher average plate velocities (Figure 6d). This behavior hints at the possibility that grain growth stabilizes subduction zones, favoring persistence, and that of grain reduction to cause slab breakoff. Alternatively, grain growth favor thicker lithospheres, and therefore higher negative buoyancy of slabs (although this is not evident in Figure 5f). Grain growth and grain reduction are not dynamic opposites, and they do not need to have a symmetrical and opposite effect in the convection diagnostics. Eq. 2 shows this assymmetry in the calculation. Furthermore, grain reduction can only occur in areas with high dislocation creep, and grain sizes will only affect diffusion creep. In chaotic systems (i.e., high Ra), assuming that high grain reduction will aid plate tectonics, and grain growth impede it, is not warranted.

When considering the time dependence of the models (supplementary video SV1, see also Figure 1g,h), processes other than subduction creation hint to the reasons of this duplicity in behavior of k and f_G. Indeed, supplementary video SV1 shows the creation of a subduction zone via lithospheric 'scar' activation (this scar, in particular, corresponds to a failed rift), but also its cessation due to slab breakoff. In fact, in models with high grain reduction, reactivation of weak zones was a relatively rare phenomenon, while breakoff due to lithospheric weakness is more common. All in all, subduction zones are more numerous in models with high grain reduction, but also their stability is smaller. As mentioned in section 2, we chose the smaller option of the p values. We admit that a higher value of p may produce stronger grain-size dependence in the lithosphere, but this may lead to an even weaker, more fragmented subduction, as observed elsewhere (Schierjott et al., 2020; Gerya et al., 2021).

4.2. Limitations

Determining the precise effects of GSE parameters in real systems must be done carefully and our models should not be interpreted further than what their design allows us. Our activation parameters, particularly activation energies, are relatively small compared to laboratory measurements (Kohlstedt and Hansen, 2015). We kept the activation energy for grain growth between the activation energies of diffusion creep and dislocation creep, as other studies have suggested (Schierjott et al., 2020), but that also meant an activation energy for grain growth below what has been measured experimentally. In turn we are confident that our results are relevant for the lower mantle, since the lower mantle features low viscosity contrasts (Yang and Gurnis, 2016), but these discrepancies between our parameters and the laboratory values could influence results, particularly in the lithosphere-asthenosphere boundary. In the latter case, the null hypothesis should be that higher creep activation energies stiffen the lithosphere, making the tectonic regime even more dependent on the yield stress.

As stated in the introduction, the main evidence for grain reduction by deformation is found in shear zones. In our work, however, resolution limitations preclude the detailed investigation of narrow shear structures, and therefore we are limited to analyze our data in terms of broad trends. Some regional geodynamic models, nonetheless, suggest that many of our findings are robust and we expect them to hold on smaller crustal-to-lithospheric scales. For example, recent regional models show the same distribution of dislocation creep and reduced grain size in mid-ocean ridges and subduction zones when compared to our global models (Gerya et al., 2021; Ruh et al., 2022).

The simplicity of our models allows us to systematically isolate the effects of GSE. However, this implies that our calculations miss several complexities of planetary mantle convection. In particular, the lack of chemical heterogeneity precludes any evaluation of important phenomena that can influence grain growth and plate tectonics such as melting or Zener pinning (Katz et al., 2022; Bercovici and Ricard, 2012). In addition, our yield stress approximation is a highly simplified form of mechanisms such as the Peierls

Creep, which should affect and be affected by GSE (Hansen et al., 2019). Future work should focus on elucidating the effects of these phenomena in models with GSE.

4.3. Implications for early Earth and Venus

When considering Earth-like k and f_G parameters (which would correspond to the higher end of k here considered, as well as a strong temperature-dependence of f_G, see Table 1), high grain reduction at lithospheric depths favors a narrow transition between stagnant lid and mobile lid. Assuming that our change in yield stress is a valid proxy for the change of the strength of the lithosphere with time (as suggested by Jain et al. (2022)), this narrow transition could imply a relatively quick change between Archean-style vertical tectonics and horizontal motion of lithospheric plates, which would be in agreement with isotopic data that found this transition occurring between 3.8 and 3.6 Ga (Bauer et al., 2020). If this was the case, the Earth may have never experienced episodic tectonics.

On Venus, however, higher surface temperatures may favor faster grain growth and less grain reduction (lower stresses), therefore enabling the episodic regime (Armann and Tackley, 2012). Nonetheless, the differences in the GSE between Earth and Venus today do not arise from intrinsically different GSE parameters (if significant) assuming a similar composition between Earth and Venus (e.g., Rolf et al., 2022), but likely from surface temperature differences and consequently different rates of grain growth (Bercovici and Ricard, 2014). Preliminary models by Landuyt and Bercovici (2009), Bercovici and Ricard (2014), or Foley and Driscoll (2016) (among others) do hint to the feasibility of this hypothesis. However, these works lack a self-consistent dynamical approach and/or composite rheology, and our results suggest that more specific models featuring different surface temperatures with composite rheology and GSE are needed to properly address this issue.

Nonetheless, models including more complex phenomena and realistic parameters may obscure some of the effects detected here. A puzzling phenomenon are the differences between the works of Schierjott et al. (2020), Paul et al. (2024) and ours. These three works present similar grain size evolution treatment but reach a different conclusion regarding self-regulation of the rheological properties. While Schierjott et al. (2020) and our models show regulation of viscosity at the expense of changing grain size (Figure 3; see also Okamoto and Hiraga, 2024), Paul et al. (2024) finds a near-constant grain size with changing viscosity. The values of Paul et al. (2024) are closer to the latest experimental values for bridgmanite, but our models show that the self-regulation depends on grain reduction and occur at all values of k (which is responsible for the absolute grain size). In turn, very specific (Earth-like) models include many other phenomena that affect cooling of the planet and/or grain size (melting, phase transitions...) which could also affect this regulation.

Whether mantle convection in Earth has been able to effectively regulate grain size or/and viscosity remains an open question with important implications. On the one hand, grain size remains important for considerations other than those studied here: incipient melting and transport depend on the surface of grains related to their volume (Philpotts and Ague, 2022; Katz et al., 2022), for example. Similar grain sizes imply similar behavior of the melt-generating asthenosphere in the past. On the other hand, if viscosity of the mantle has been similar during Earth's history, convection-related changes such as the onset of plate tectonics must have happened early on Earth's history. This latter sentence makes our models consistent with early transitions to plate tectonics on Earth (e.g., Bauer et al., 2020), while interpretations claiming a more recent starting point of plate tectonics (e.g., Stern, 2018) may be more consistent with Paul et al. (2024), since they require a system able to change its internal properties.

Regardless of which exact parameter values are representative of the Earth, we are confident that our models do reflect the systematic changes that planetary mantle convection undergoes with changing GSE parameters. Our models show that considering GSE imprints a new array of behaviors and diagnostic changes that can only be reproduced by models without GSE when considering composite rheology (e.g. Arnould et al., 2023), and only if the grain growth/reduction parameters are assumed to be in the low side of the array here explored (Figure 7, supplementary Figure S1), which would not be the case of Earth, for example. Moreover, simplified models of GSE may be overstating the effect of grain size on lithospheric strength for subduction creation, while ignoring its potential for subduction cessation. Likewise, healing by grain growth may preclude subduction creation, but once created may favor its persistence.

5. conclusions

To summarize, our models show the following systematics for the different tectonic regimes and the transitions between them:

- increasing neither grain growth nor grain reduction substantially changes the critical yield stress of the lithosphere at which the transition to the stagnant-lid regime occurs. The effects within one regime are nonetheless stark.

- Increasing grain growth and/or grain reduction efficiently promotes lower internal temperatures. High grain growth limits the transfer of heat from the core to the mantle; while high grain reduction favors cooling by tectonic recycling.

- For Earth, the transition between stagnant lid and mobile lid may have not gone through an episodic period, while on Venus the episodic regime may have been favored due to higher surface temperatures, lower grain reduction and higher grain growth, but further work is needed to resolve this question.

6. Author contributions: CRediT

Antonio Manjón/Cabeza Córdoba: Conceptualization; Software; Formal analysis; Validation; Visualization; Investigation; Methodology; Writing-original draft; Writing-review and editing. Tobias Rolf: Conceptualization; Software; Funding acquisition; Investigation; Project administration; Writing-review and editing. Maëlis Arnould: Conceptualization; Software; Writing-review and editing.

7. Funding Sources

The authors acknowledge support from the Research Council of Norway through its Centres of Excellence scheme, grant number 223272 (Centre for

Earth Evolution and Dynamics), and through the Young Talents scheme (grant 276032 to TR, PLATONICS).

All calculations were run on SAGA (Uninett Sigma2 project nn9010k) and benefited from data storage on NIRD (Uninett Sigma2 project NS9010K). AM benefited from the Margarita Salas grant by the “plan de recuperación” of the Government of Spain.

References

Alisic, L., Gurnis, M., Stadler, G., Burstedde, C., Wilcox, L.C., Ghattas, O., 2010. Slab stress and strain rate as constraints on global mantle flow. Geophysical Research Letters 37, n/a–n/a. URL: http://doi.wiley.com/10.1029/2010GL045312, doi:10.1029/2010GL045312.

Ardell, A., 1972. On the coarsening of grain boundary precipitates. Acta Metallurgica 20, 601–609. URL: https://linkinghub.elsevier.com/retrieve/pii/0001616072900156, doi:10.1016/0001-6160(72)90015-6.

Armann, M., Tackley, P.J., 2012. Simulating the thermochemical magmatic and tectonic evolution of venus's mantle and lithosphere: Two-dimensional models. Journal of Geophysical Research: Planets 117, E12003. URL: http://doi.wiley.com/10.1029/2012JE004231, doi:10.1029/2012JE004231.

Arnould, M., Rolf, T., Manjón-Cabeza Córdoba, A., 2023. Effects of composite rheology on plate-like behavior in global-scale mantle convection. Geophysical Research Letters 50. URL: https://agupubs.onlinelibrary.wiley.com/doi/10.1029/2023GL104146, doi:10.1029/2023GL104146.

Austin, N.J., Evans, B., 2007. Paleowattmeters: A scaling relation for dynamically recrystallized grain size. Geology 35, 343–346. doi:10.1130/G23244A.1.

Bauer, A., Reimink, J., Chacko, T., Foley, B., Shirey, S., Pearson, D., 2020. Hafnium isotopes in zircons document the gradual onset of mobile-lid tectonics. Geochemical Perspectives Letters 14, 1–6. URL: http://www.geochemicalperspectivesletters.org/article2015, doi:10.7185/geochemlet.2015.

Bercovici, D., Ricard, Y., 2012. Mechanisms for the generation of plate tectonics by two-phase grain-damage and pinning. Physics of the Earth and Planetary Interiors 202-203, 27–55. URL: http://dx.doi.org/10.1016/j.pepi.2012.05.003, doi:10.1016/j.pepi.2012.05.003.

Bercovici, D., Ricard, Y., 2014. Plate tectonics, damage and inheritance. Nature 508, 513–516. doi:10.1038/nature13072.

Bercovici, D., Ricard, Y., 2016. Grain-damage hysteresis and plate tectonic states. Physics of the Earth and Planetary Interiors 253, 31–47. URL: http://dx.doi.org/10.1016/j.pepi.2016.01.005, doi:10.1016/j.pepi.2016.01.005.

Bercovici, D., Tackley, P.J., Ricard, Y., 2015. The Generation of Plate Tectonics from Mantle Dynamics. volume 7. Elsevier B.V. URL: http://dx.doi.org/10.1016/B978-0-444-53802-4.00135-4, doi:10.1016/B978-0-444-53802-4.00135-4.

Brace, W.F., Kohlstedt, D.L., 1980. Limits on lithospheric stress imposed by laboratory experiments. Journal of Geophysical Research: Solid Earth 85, 6248–6252. URL: http://doi.wiley.com/10.1029/JB085iB11p06248, doi:10.1029/JB085iB11p06248.

Byrne, P.K., Ghail, R.C., Şengör, A.M., James, P.B., Klimczak, C., Solomon, S.C., 2021. A globally fragmented and mobile lithosphere on venus. Proceedings of the National Academy of Sciences of the United States of America 118, e2025919118. doi:10.1073/pnas.2025919118.

Christensen, U.R., Yuen, D.A., 1985. Layered convection induced by phase transitions. Journal of Geophysical Research 90, 10291. URL: http://doi.wiley.com/10.1029/JB090iB12p10291, doi:10.1029/JB090iB12p10291.

Crameri, F., Shephard, G.E., Conrad, C.P., 2019. Plate Tectonics. Elsevier. URL: https://linkinghub.elsevier.com/retrieve/pii/B9780124095489123930, doi:10.1016/B978-0-12-409548-9.12393-0.

Dannberg, J., Eilon, Z., Faul, U., Gassmöller, R., Moulik, P., Myhill, R., 2017. The importance of grain size to mantle dynamics and seismological observations. Geochemistry, Geophysics, Geosystems 18, 3034–3061. URL:

https://onlinelibrary.wiley.com/doi/10.1002/2017GC006944, doi:10.1002/2017GC006944.

Foley, B.J., 2015. The role of plate tectonic-climate coupling and exposed land area in the development of habitable climates on rocky planets. Astrophysical Journal 812, 36. URL: http://dx.doi.org/10.1088/0004-637X/812/1/36, doi:10.1088/0004-637X/812/1/36.

Foley, B.J., Bercovici, D., 2014. Scaling laws for convection with temperature-dependent viscosity and grain-damage. Geophysical Journal International 199, 580–603. doi:10.1093/gji/ggu275.

Foley, B.J., Driscoll, P.E., 2016. Whole planet coupling between climate, mantle, and core: Implications for rocky planet evolution. Geochemistry, Geophysics, Geosystems 17, 1885–1914. URL: https://onlinelibrary.wiley.com/doi/10.1002/2015GC006210, doi:10.1002/2015GC006210.

Foley, B.J., Rizo, H., 2017. Long-term preservation of early formed mantle heterogeneity by mobile lid convection: Importance of grainsize evolution. Earth and Planetary Science Letters 475, 94–105. URL: http://dx.doi.org/10.1016/j.epsl.2017.07.031, doi:10.1016/j.epsl.2017.07.031.

Fuchs, L., Becker, T.W., 2019. Role of strain-dependent weakening memory on the style of mantle convection and plate boundary stability. Geophysical Journal International 218, 601–618. doi:10.1093/gji/ggz167.

Fuchs, L., Becker, T.W., 2022. On the role of rheological memory for convection-driven plate reorganizations. Geophysical Research Letters 49, e2022GL099574. URL: https://agupubs.onlinelibrary.wiley.com/doi/10.1029/2022GL099574, doi:10.1029/2022GL099574.

Gerya, T.V., Bercovici, D., Becker, T.W., 2021. Dynamic slab segmentation due to brittle–ductile damage in the outer rise. Nature 599, 245–250. doi:10.1038/s41586-021-03937-x.

Hansen, L., Zimmerman, M., Dillman, A., Kohlstedt, D., 2012. Strain localization in olivine aggregates at high temperature: A laboratory comparison of constant-strain-rate and constant-stress boundary conditions. Earth and Planetary Science Letters 333-334, 134–145. URL: http://dx.doi.org/10.1016/j.epsl.2012.04.016 https://linkinghub.elsevier.com/retrieve/pii/S0012821X12001835, doi:10.1016/j.epsl.2012.04.016.

Hansen, L.N., Kumamoto, K.M., Thom, C.A., Wallis, D., Durham, W.B., Goldsby, D.L., Breithaupt, T., Meyers, C.D., Kohlstedt, D.L., 2019. Low-temperature plasticity in olivine: Grain size, strain hardening, and the strength of the lithosphere. Journal of Geophysical Research: Solid Earth 124, 5427–5449. doi:10.1029/2018JB016736.

Hirth, G., Kohlstedt, D., 2003. Rheology of the upper mantle and the mantle wedge: A view from the experimentalists. volume 138. pp. 83–105. URL: https://onlinelibrary.wiley.com/doi/10.1029/138GM06, doi:10.1029/138GM06.

Hirth, G., Kohlstedt, D.L., 2015. The stress dependence of olivine creep rate: Implications for extrapolation of lab data and interpretation of recrystallized grain size. Earth and Planetary Science Letters 418, 20–26. URL: http://dx.doi.org/10.1016/j.epsl.2015.02.013, doi:10.1016/j.epsl.2015.02.013.

Jain, C., Korenaga, J., Karato, S., 2018. On the grain size sensitivity of olivine rheology. Journal of Geophysical Research: Solid Earth 123, 674–688. URL: https://agupubs.onlinelibrary.wiley.com/doi/10.1002/2017JB014847, doi:10.1002/2017JB014847.

Jain, C., Korenaga, J., Karato, S., 2019. Global analysis of experimental data on the rheology of olivine aggregates. Journal of Geophysical Research: Solid Earth 124, 310–334. URL: https://agupubs.onlinelibrary.wiley.com/doi/10.1029/2018JB016558, doi:10.1029/2018JB016558.

Jain, C., Rozel, A.B., van Hunen, J., Chin, E.J., Manjón-Cabeza Córdoba, A., 2022. Building archean cratonic roots. Frontiers in Earth Science 10. doi:10.3389/feart.2022.966397.

Karato, S., Wu, P., 1993. Rheology of the upper mantle: A synthesis. Science 260, 771–778. URL: https://www.science.org/doi/10.1126/science.260.5109.771, doi:10.1126/science.260.5109.771.

Karato, S.i., 2010. Rheology of the earth's mantle: A historical review. Gondwana Research 18, 17–45. URL: https://linkinghub.elsevier.com/retrieve/pii/S1342937X1000064X, doi:10.1016/j.gr.2010.03.004.

Katz, R.F., Jones, D.W.R., Rudge, J.F., Keller, T., 2022. Physics of melt extraction from the mantle: Speed and style. Annual Review of Earth and Planetary Sciences 50, 507–540. URL: https://www.annualreviews.org/doi/10.1146/annurev-earth-032320-083704, doi:10.1146/annurev-earth-032320-083704.

Kohlstedt, D., Hansen, L., 2015. Constitutive Equations, Rheological Behavior, and Viscosity of Rocks. Elsevier. volume 2. pp. 441–472. URL: https://linkinghub.elsevier.com/retrieve/pii/B9780444538024000427, doi:10.1016/B978-0-444-53802-4.00042-7.

Korenaga, J., 2017. Pitfalls in modeling mantle convection with internal heat production. Journal of Geophysical Research: Solid Earth 122, 4064–4085. URL: http://doi.wiley.com/10.1002/2016JB013850, doi:10.1002/2016JB013850.

Landuyt, W., Bercovici, D., 2009. Variations in planetary convection via the effect of climate on damage. Earth and Planetary Science Letters 277, 29–37. URL: http://dx.doi.org/10.1016/j.epsl.2008.09.034 https://linkinghub.elsevier.com/retrieve/pii/S0012821X08006420, doi:10.1016/j.epsl.2008.09.034.

Lourenço, D.L., Rozel, A.B., 2023. The Past and the Future of Plate Tectonics and Other Tectonic Regimes. Elsevier. pp. 181–196. URL:

https://linkinghub.elsevier.com/retrieve/pii/B9780323857338000044, doi:10.1016/B978-0-323-85733-8.00004-4.

Mulyukova, E., Bercovici, D., 2023. The Physics and Origin of Plate Tectonics From Grains to Global Scales. Elsevier Inc. URL: http://dx.doi.org/10.1016/B978-0-323-85733-8.00015-9, doi:10.1016/b978-0-323-85733-8.00015-9.

Newman, J., Drury, M.R., 2010. Control of shear zone location and thickness by initial grain size variations in upper mantle peridotites. Journal of Structural Geology 32, 832–842. URL: http://dx.doi.org/10.1016/j.jsg.2010.06.001 https://linkinghub.elsevier.com/retrieve/pii/S0191814110000921, doi:10.1016/j.jsg.2010.06.001.

Okamoto, A., Hiraga, T., 2024. A common diffusional mechanism for creep and grain growth in polymineralic rocks: Application to lower mantle viscosity estimates. Journal of Geophysical Research: Solid Earth 129, e2023JB027803. URL: https://agupubs.onlinelibrary.wiley.com/doi/10.1029/2023JB027803, doi:10.1029/2023JB027803.

Paul, J., Golabek, G.J., Rozel, A.B., Tackley, P.J., Katsura, T., Fei, H., 2024. Effect of bridgmanite-ferropericlase grain size evolution on earth's average mantle viscosity: implications for mantle convection in early and present-day earth. Progress in Earth and Planetary Science 11. doi:10.1186/s40645-024-00658-3.

Philpotts, A.R., Ague, J.J., 2022. Principles of Igneous and Metamorphic Petrology. Cambridge University Press. URL: https://www.cambridge.org/highereducation/product/9781108631419/book, doi:10.1017/9781108631419.

Platt, J., Behr, W., 2011. Lithospheric shear zones as constant stress experiments. Geology 39, 127–130. URL: http://pubs.geoscienceworld.org/geology/article/39/2/127/130486/Lithospheric-she doi:10.1130/G31561.1.

Rolf, T., Weller, M., Gülcher, A., Byrne, P., O'Rourke, J.G., Herrick, R., Bjonnes, E., Davaille, A., Ghail, R., Gillmann, C., Plesa, A.C., Smrekar, S., 2022. Dynamics and evolution of venus' mantle through time. Space Science Reviews 218, 70. URL: http://dx.doi.org/10.1007/s11214-022-00937-9 https://link.springer.com/10.1007/s11214-022-00937-9, doi:10.1007/s11214-022-00937-9.

Rozel, A., 2012. Impact of grain size on the convection of terrestrial planets. Geochemistry, Geophysics, Geosystems 13, Q10020. URL: http://doi.wiley.com/10.1029/2012GC004282, doi:10.1029/2012GC004282.

Rozel, A., Golabek, G.J., Näf, R., Tackley, P.J., 2015. Formation of ridges in a stable lithosphere in mantle convection models with a viscoplastic rheology. Geophysical Research Letters 42, 4770–4777. URL: http://doi.wiley.com/10.1002/2015GL063483, doi:10.1002/2015GL063483.

Rozel, A., Ricard, Y., Bercovici, D., 2011. A thermodynamically self-consistent damage equation for grain size evolution during dynamic recrystallization. Geophysical Journal International 184, 719–728. doi:10.1111/j.1365-246X.2010.04875.x.

Ruh, J.B., Tokle, L., Behr, W.M., 2022. Grain-size-evolution controls on lithospheric weakening during continental rifting. Nature Geoscience 15, 585–590. URL: https://www.nature.com/articles/s41561-022-00964-9, doi:10.1038/s41561-022-00964-9.

Schierjott, J.C., Rozel, A., Tackley, P., 2020. On the self-regulating effect of grain size evolution in mantle convection models: Application to thermochemical piles. Solid Earth 11, 959–982. doi:10.5194/se-11-959-2020.

Solomatov, V., El-Khozondar, R., Tikare, V., 2002. Grain size in the lower mantle: constraints from numerical modeling of grain growth in two-phase systems. Physics of the Earth and Planetary Interiors 129, 265–282. URL: https://linkinghub.elsevier.com/retrieve/pii/S0031920101002953, doi:10.1016/S0031-9201(01)00295-3.

Solomatov, V.S., 1996. Can hotter mantle have a larger viscosity? Geophysical Research Letters 23, 937–940. URL: http://doi.wiley.com/10.1029/96GL00724, doi:10.1029/96GL00724.

Solomatov, V.S., 2001. Grain size-dependent viscosity convection and the thermal evolution of the earth. Earth and Planetary Science Letters 191, 203–212. doi:10.1016/S0012-821X(01)00426-5.

Stern, R.J., 2018. The evolution of plate tectonics. Philosophical Transactions of the Royal Society A: Mathematical, Physical and Engineering Sciences 376. doi:10.1098/rsta.2017.0406.

Stern, R.J., Gerya, T., Tackley, P.J., 2018. Stagnant lid tectonics: Perspectives from silicate planets, dwarf planets, large moons, and large asteroids. Geoscience Frontiers 9, 103–119. URL: https://doi.org/10.1016/j.gsf.2017.06.004, doi:10.1016/j.gsf.2017.06.004.

Tackley, P.J., 2000. Self-consistent generation of tectonic plates in time-dependent, three-dimensional mantle convection simulations. Geochemistry, Geophysics, Geosystems 1, 1021. URL: http://doi.wiley.com/10.1029/2000GC000036, doi:10.1029/2000GC000036.

Tackley, P.J., 2008. Modelling compressible mantle convection with large viscosity contrasts in a three-dimensional spherical shell using the yin-yang grid. Physics of the Earth and Planetary Interiors 171, 7–18. URL: https://linkinghub.elsevier.com/retrieve/pii/S0031920108002276, doi:10.1016/j.pepi.2008.08.005.

Tian, J., Tackley, P.J., Lourenço, D.L., 2023. The tectonics and volcanism of venus: New modes facilitated by realistic crustal rheology and intrusive magmatism. Icarus 399, 115539. URL: https://linkinghub.elsevier.com/retrieve/pii/S0019103523001161, doi:10.1016/j.icarus.2023.115539.

Tosi, N., Padovan, S., 2021. Mercury, Moon, Mars: Surface Expressions of Mantle Convection and interior Evolution of Stagnant-Lid Bodies. first ed.. John Wiley & Sons, Ltd. pp. 455–489. URL: https://onlinelibrary.wiley.com/doi/10.1002/9781119528609.ch17, doi:10.1002/9781119528609.ch17.

Trompert, R., Hansen, U., 1998. Mantle convection simulations with rheologies that generate plate-like behaviour. Nature 395, 686–689. URL: http://www.nature.com/articles/27185, doi:10.1038/27185.

Turcotte, D., Schubert, G., 2014. Geodynamics. 3rd ed., Cambridge University Press.

Uppalapati, S., Rolf, T., Crameri, F., Werner, S.C., 2020. Dynamics of lithospheric overturns and implications for venus's surface. Journal of Geophysical Research: Planets 125, 1–29. URL: https://onlinelibrary.wiley.com/doi/10.1029/2019JE006258, doi:10.1029/2019JE006258.

Vauchez, A., Tommasi, A., Mainprice, D., 2012. Faults (shear zones) in the earth's mantle. Tectonophysics 558-559, 1–27. URL: http://dx.doi.org/10.1016/j.tecto.2012.06.006 https://linkinghub.elsevier.com/retrieve/pii/S0040195112003125, doi:10.1016/j.tecto.2012.06.006.

Wagner, C., 1961. Theorie der alterung von niederschlägen durch umlösen. Zeitschrift für Elektrochemie 65, 581–591.

Warren, J.M., Hansen, L.N., 2023. Ductile deformation of the lithospheric mantle. Annual Review of Earth and Planetary Sciences 51, 581–609. URL: https://www.annualreviews.org/doi/10.1146/annurev-earth-031621-063756, doi:10.1146/annurev-earth-031621-063756.

Warren, J.M., Hirth, G., 2006. Grain size sensitive deformation mechanisms in naturally deformed peridotites. Earth and Planetary Science Letters 248, 438–450. URL: https://linkinghub.elsevier.com/retrieve/pii/S0012821X06004225, doi:10.1016/j.epsl.2006.06.006.

Weller, M.B., Lenardic, A., 2012. Hysteresis in mantle convection: Plate tectonics systems. Geophysical Research Letters 39, L10202. URL: http://doi.wiley.com/10.1029/2012GL051232, doi:10.1029/2012GL051232.

Yang, T., Gurnis, M., 2016. Dynamic topography, gravity and the role of lateral viscosity variations from inversion of global mantle flow. Geophysical Journal International 207, 1186–1202. URL: https://academic.oup.com/gji/article-lookup/doi/10.1093/gji/ggw335, doi:10.1093/gji/ggw335.

Supplementary Material for "Grain size evolution in mantle convection models promotes continuous rather than episodic tectonics"

Antonio Manjón-Cabeza Córdoba[a,b,c], Tobias Rolf[b,d], Maëlis Arnould[e]

[a] *University College London, Department of Earth Sciences, 5 Gower Place, London, WC1E 6BS, U.K.*
[b] *The Centre for Earth Evolution and Dynamics (CEED), Universitetet i Oslo, P.O. Box 1028 Blindern, Oslo, N-0315, Norway*
[c] *Instituto Andaluz de Ciencias de la Tierra (UGR-CSIC), Avda. de las Palmeras 4, Granada, 18100, Spain*
[d] *Institute of Geophysics, University of Münster, Corrensstrasse 24, Münster, 48149, Germany*
[e] *University of Lyon, UCBL, ENSL, UJM, CNRS 5276, Laboratoire de Géologie de Lyon - Terre, Plànetes, Environnement, Camps de la DOUA Bâtiement Géode 2 Rue Raphaël Dubois, Lyon, 69622, France*

Contents of this file

Email address: a.cordoba@ucl.ac.uk (Antonio Manjón-Cabeza Córdoba)

1. Introduction

Here we present the supplementary information for our paper "Grain size evolution in mantle convection models promotes continuous rather than episodic tectonics". Table S1 shows a summary of the models run for this work and the specific nondimensional parameters varied in each one. Figure S3 shows models with constant grain size compared to the reference case (see text for details). The caption for supplementary video SV1 shows a short description of the process depicted in SV1 (attached separately).

2. Table S1

List of models used in this paper. CGS stands for Constant Grain Size. For the rest of the parameter symbols and interpretation, see Table 1 and main text.

Model ID	K	f_G	YS	Model ID	K	f_G	YS
MRA23-16	$5{\times}10^{-26}$	10^{-6}	$5{\times}10^3$	MRA23-61	$5{\times}10^{-25}$	10^{-6}	10^5
MRA23-22	$5{\times}10^{-26}$	10^{-5}-10^{-7}	$5{\times}10^3$	MRA23-62	$5{\times}10^{-25}$	10^{-6}	$3{\times}10^5$
MRA23-23	$5{\times}10^{-26}$	10^{-4}-10^{-7}	$5{\times}10^3$	MRA23-63	$5{\times}10^{-25}$	10^{-6}	10^6
MRA23-24	$5{\times}10^{-26}$	10^{-3}-10^{-7}	$5{\times}10^3$	MRA23-64	$5{\times}10^{-27}$	10^{-6}	$5{\times}10^3$
MRA23-26	$5{\times}10^{-26}$	10^{-6}	10^3	MRA23-65	$5{\times}10^{-24}$	10^{-6}	$5{\times}10^3$
MRA23-28	10^{-25}	10^{-4}-10^{-7}	$5{\times}10^3$	MRA23-66	$5{\times}10^{-26}$	10^{-4}	$2{\times}10^4$
MRA23-29	$5{\times}10^{-25}$	10^{-4}-10^{-7}	$5{\times}10^3$	MRA23-67	$5{\times}10^{-25}$	10^{-6}	$2{\times}10^4$
MRA23-36	$5{\times}10^{-26}$	10^{-6}	10^4	MRA23-68	$5{\times}10^{-26}$	10^{-4}-10^{-7}	$2{\times}10^4$
MRA23-37	$5{\times}10^{-26}$	10^{-6}	$2{\times}10^4$	MRA23-69	$5{\times}10^{-26}$	10^{-4}	10^4
MRA23-39	10^{-26}	10^{-4}-10^{-7}	$5{\times}10^3$	MRA23-70	$5{\times}10^{-25}$	10^{-6}	10^4
MRA23-40	10^{-26}	10^{-6}	$5{\times}10^3$	MRA23-71	$5{\times}10^{-26}$	10^{-4}-10^{-7}	10^4
MRA23-41	10^{-25}	10^{-6}	$5{\times}10^3$	MRA23-72	$5{\times}10^{-26}$	10^{-6}	$5{\times}10^4$
MRA23-42	$5{\times}10^{-25}$	10^{-6}	$5{\times}10^3$	MRA23-73	$5{\times}10^{-26}$	10^{-4}-10^{-7}	$5{\times}10^4$
MRA23-47	$5{\times}10^{-26}$	10^{-7}	$5{\times}10^3$	MRA23-74	$5{\times}10^{-26}$	10^{-4}	$5{\times}10^4$
MRA23-48	$5{\times}10^{-26}$	10^{-5}	$5{\times}10^3$	MRA23-75	$5{\times}10^{-25}$	10^{-6}	$5{\times}10^4$
MRA23-49	$5{\times}10^{-26}$	10^{-6}	10^5	MRA23-76	$5{\times}10^{-26}$	10^{-6}	$2{\times}10^5$
MRA23-50	$5{\times}10^{-26}$	10^{-6}	10^6	MRA23-77	$5{\times}10^{-26}$	10^{-4}-10^{-7}	$2{\times}10^5$
MRA23-52	$5{\times}10^{-26}$	10^{-4}	$5{\times}10^3$	MRA23-78	$5{\times}10^{-26}$	10^{-4}	$2{\times}10^5$
MRA23-53	$5{\times}10^{-26}$	10^{-2}-10^{-7}	$5{\times}10^3$	MRA23-79	$5{\times}10^{-25}$	10^{-6}	$2{\times}10^5$
MRA23-54	$5{\times}10^{-26}$	10^{-6}	$3{\times}10^5$	MRA23-16_5	CGS	CGS	$5{\times}10^3$
MRA23-55	$5{\times}10^{-26}$	10^{-4}-10^{-7}	10^5	MRA23-16_1	CGS	CGS	$5{\times}10^3$
MRA23-56	$5{\times}10^{-26}$	10^{-4}-10^{-7}	$3{\times}10^5$	MRA23-16_2	CGS	CGS	$5{\times}10^3$
MRA23-57	$5{\times}10^{-26}$	10^{-4}-10^{-7}	10^6	MRA23-37_1	CGS	CGS	10^4
MRA23-58	$5{\times}10^{-26}$	10^{-4}	10^5	MRA23-49_1	CGS	CGS	10^5
MRA23-59	$5{\times}10^{-26}$	10^{-4}	$3{\times}10^5$	MRA23-54_1	CGS	CGS	$3{\times}10^5$
MRA23-60	$5{\times}10^{-26}$	10^{-4}	10^6	MRA23-72_1	CGS	CGS	$5{\times}10^4$

3. Figure S1

Comparison of radial profiles of the reference case (see main text) and three different cases with constant grain size. (a) Temperature profile. (b) Viscosity profile. Note that an average grain size of 10^8 reproduces the average characteristics of the reference case (low grain growth and grain reduction) except for the bottom boundary layer, where viscosity is lower for the case of constant grain size. This value depends completely of D_0 (table S1) and is physically meaningless (i.e., can be added to a constant prefactor in equation 1, main text).

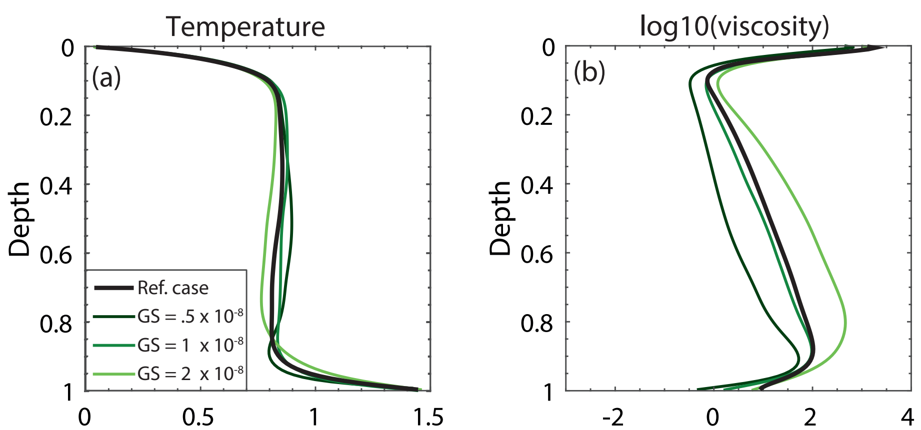

4. Caption for Supplementary Video SV1

Animation of the inheritance process in a model with GSE. (clockwise from top-left) Temperature field, viscosity field, grain size field, and deformation mechanism field. For color scales, see Figure 1 in the main text.

A lithospheric scar (zone of low viscosity and low grain size) from a previous deformation event is reactivated and a subduction zone is created. In turn, this subduction zone is short-lived due to slab break-off, but another 'scar' is left in the lithosphere.